

ARTICLE

Received 26 Nov 2013 | Accepted 6 Jun 2014 | Published 14 Jul 2014

DOI: 10.1038/ncomms5332

OPEN

Local mapping of detector response for reliable quantum state estimation

Merlin Cooper¹, Michał Karpiński¹ & Brian J. Smith¹

Improved measurement techniques are central to technological development and foundational scientific exploration. Quantum physics relies on detectors sensitive to non-classical features of systems, enabling precise tests of physical laws and quantum-enhanced technologies including precision measurement and secure communications. Accurate detector response calibration for quantum-scale inputs is key to future research and development in these cognate areas. To address this requirement, quantum detector tomography has been recently introduced. However, this technique becomes increasingly challenging as the complexity of the detector response and input space grow in a number of measurement outcomes and required probe states, leading to further demands on experiments and data analysis. Here we present an experimental implementation of a versatile, alternative characterization technique to address many-outcome quantum detectors that limits the input calibration region and does not involve numerical post processing. To demonstrate the applicability of this approach, the calibrated detector is subsequently used to estimate non-classical photon number states.

¹Clarendon Laboratory, University of Oxford, Parks Road, Oxford OX1 3PU, UK. Correspondence and requests for materials should be addressed to M.C. (email: m.cooper1@physics.ox.ac.uk).

Experimental quantum optics relies on the ability to create, manipulate and measure the state of the light field for applications ranging from fundamental scientific research^{1–4} to the development of quantum technologies that harness the non-classical behaviour of light^{5–8}. Methods to characterize each step of a quantum experiment are crucial to ensure appropriate evaluation of tests of theoretical predictions and desired device operation. Well-developed techniques for quantum state estimation (QSE)^{9–11} and quantum process tomography^{12–15} rely on accurate knowledge of the detector response. Only recently has the independent characterization of quantum detectors with few outcomes been experimentally demonstrated by means of quantum detector tomography (QDT)^{16–22}.

Complete characterization of the detector response through QDT becomes increasingly demanding as the number of detector outcomes grows. The primary roadblocks arise from the need to acquire and analyse expanded data sets to extract the mathematical operators associated with each measurement outcome, which becomes intractable with current experimental and computational capacity. This is due to experimental instability over the time required to collect sufficient data, and the size of the numerical inversion problem in terms of the number of distinct measurement outcomes and unavoidable statistical noise that can distort rare detection events²³.

Here we present an experimental demonstration of an alternative approach to QSE and QDT, known as the fitting of data patterns (FDP)^{24,25}, which enables calibration of detectors with a sizable number of outcomes and their subsequent use in state estimation. This technique does not extract the complete set of operators that describe the detector, but rather uses the raw measurement outcome distributions for known input states as the detector calibration—negating the need for post processing. The approach limits the input state space to a finite region of interest set by the experimenter independent of the detector behaviour. We apply the FDP method to a balanced homodyne detector (BHD)^{9,11}, a central resource in a broad class of quantum optical experiments^{11,26}, which is yet to be independently characterized. The BHD employed here has more than 150 outcomes, which is an order of magnitude more than any quantum detector characterized to date. To demonstrate the FDP method as a tool for complex detector calibration and QSE, we subsequently present QSE of non-classical states of light using the independently calibrated BHD.

Results

QSE with a calibrated detector. In quantum theory, the detector response is mathematically represented by its positive operator-valued measure (POVM) comprising a set of positive operators $\{\pi_n\}$, with $n = 1, 2, \dots, N$, labelling the measurement outcomes. The probability for detector outcome n given input state σ_ξ is determined by the Born rule

$$p_n^{(\xi)} = \text{Tr}(\pi_n \sigma_\xi). \quad (1)$$

QDT aims to determine the set of measurement operators $\{\pi_n\}$ by taking the experimentally estimated outcome probabilities $\{p_n^{(\xi)}\}$ for a set of known probe states $\{\sigma_\xi\}$, and inverting equation (1) (refs 16–22,27,28). To reliably invert equation (1), current QDT techniques depend on registering every measurement outcome of the detector^{17,19,22,23}, which requires an increasingly large set of probe states as the number of measurement outcomes and input state space of the detector grow. This leads to greater experimental and computational challenges for reconstruction of the complete POVM set^{17,19,22,23}. Although recent work has shown that it may be feasible to address part of the POVM in a truncated input space by

artificially limiting the number of detector outcomes²⁰, this relies on the same techniques as standard QDT. Having determined the POVM set by QDT, to reconstruct an unknown quantum state one must employ the reconstructed measurement operators within a separate QSE algorithm, for example, maximum-likelihood (ML) estimation^{29–31}. Thus, two separate algorithms (and hence two optimization procedures) are employed to perform QSE with calibrated measurements following this approach.

The FDP approach begins by recording the detector response to a set of M known input probe states $\{\sigma_\xi\}$ that span the input region of interest. Here σ_ξ is the density operator for the state labelled by $\xi = 1, 2, \dots, M$. Multiple copies of each probe state are sent to the detector and the frequency distribution $f_n^{(\xi)}$ of measurement outcomes, labelled by n , associated with input state σ_ξ , is determined as depicted in Fig. 1a. This procedure is similar to mapping the impulse response function of a linear optical system. The data pattern set $\{f_n^{(\xi)}\}$ constitutes the detector calibration within the field of view defined by the probe states. As with QDT, the FDP method relies on the ability to reliably produce a sufficient set of well-known probe states to characterize the detector response^{24,25}. However, unlike QDT, the data patterns are obtained directly from the measurement outcomes, requiring no additional analysis.

To estimate an unknown quantum state with density operator ρ using the FDP approach, many identically prepared copies of the state are measured with the calibrated detector. The frequency distribution of measurement outcomes for the unknown state $f_n^{(\rho)}$ is determined from the acquired data. The unknown state density operator is estimated as a weighted sum of the probe states

$$\rho_{\text{fdp}} = \sum_{\xi} a_{\xi} \sigma_{\xi}, \quad (2)$$

where the real-valued expansion coefficients $\{a_{\xi}\}$ are found by minimizing the functional

$$E(\{a_{\xi}\}) = \sum_n \left(f_n^{(\rho)} - \sum_{\xi} a_{\xi} f_n^{(\xi)} \right)^2 \quad (3)$$

subject to constraints $\sum_{\xi} a_{\xi} = 1$ and $\sum_{\xi} a_{\xi} \sigma_{\xi} \geq 0$, which ensure that the reconstructed operator corresponds to a physical state. The FDP algorithm can be formulated as a semi-definite convex program, which can be solved using standard software tools (see Methods). The only assumptions are that the unknown state lies within the calibration field of view defined by the probe states and can be well-represented as a weighted sum of the probe states, equation (2). Note that in the data pattern calibration and state estimation by FDP, the detector POVM $\{\pi_n\}$ is never revealed, hence the mathematical description of the measurements remains unknown to the experimentalist.

The physical origin for the FDP state estimation approach, encapsulated in the functional of equation (3), can be understood by examining the Born rule, equation (1), applied to the probe states and estimated state. Minimization of the functional in equation (3) aims to reduce the difference between the probability distribution for the unknown state, $p_n^{(\rho)} \approx f_n^{(\rho)}$, and that calculated from the estimated state $p_n^{(\rho_{\text{fdp}})} = \text{Tr}(\pi_n \rho_{\text{fdp}}) = \sum_{\xi} a_{\xi} \text{Tr}(\pi_n \sigma_{\xi}) \approx \sum_{\xi} a_{\xi} f_n^{(\xi)}$, where probabilities are approximated by their corresponding measured frequencies.

The FDP method uses an operational characterization of the detector response, encapsulated in the data pattern set $\{f_n^{(\xi)}\}$, to perform reliable QSE by minimizing only one functional, equation (3) (refs 24,25). The detector calibration consists only of the directly obtained measurement outcome distributions and

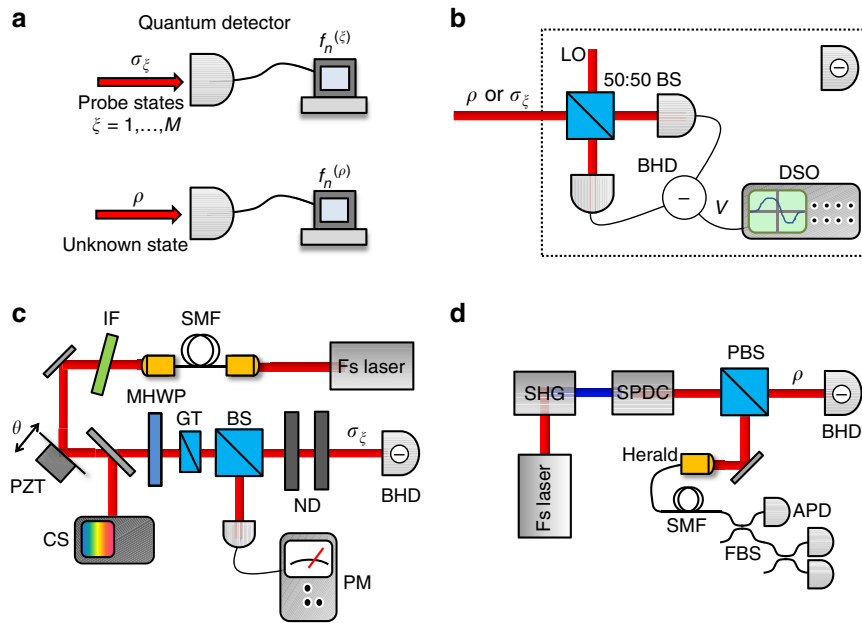


Figure 1 | FDP overview and experimental schematic. (a) Conceptual and (b–d) experimental diagrams of the FDP procedure. (a) Top: multiple copies of known probe quantum states $\{\sigma_\xi\}$ are separately measured by the unknown detector to form the data patterns $\{f_n^{(\xi)}\}$. Bottom: multiple copies of the unknown quantum state ρ to be estimated are measured giving the frequency distribution $f_n^{(\rho)}$. (b) Balanced homodyne detection: probe states $\{\sigma_\xi\}$ or unknown states ρ are combined with the local oscillator (LO) on a 50:50 beam splitter (50:50 BS). The output modes are directed to a pair of photodiodes whose photocurrents are subtracted, with the resulting difference current converted to a voltage measured with a digitizing oscilloscope (DSO)³⁹. This yields a set of voltages $\{V\}$ for each state from which the frequency distributions $\{f_n^{(\xi)}\}$ and $f_n^{(\rho)}$ are determined. (c) Probe state preparation: the output of a pulsed Ti:Sapphire laser oscillator is spatially and spectrally filtered with a single-mode fibre (SMF) and interference filter (IF). A motorized half-wave plate (MHWP) and Glan–Taylor polarizer (GT) followed by neutral density (ND) filters control the probe state amplitude, while a piezoelectric transducer (PZT) averages the phase. A calibrated power meter (PM) and compact spectrometer (CS) monitor the optical power and wavelength, respectively, to determine the probe state amplitude. (d) Fock state preparation: the Ti:Sapphire laser output is frequency doubled (SHG) to pump a spontaneous parametric downconversion source (SPDC). A spatially multiplexed detector comprising a fibre beam splitter (FBS) network and three avalanche photodiodes (APDs) enables heralding of multi-photon Fock states ρ .

thus does not require further numerical analysis. The alternative approach of performing QDT followed by QSE entails two separate optimization procedures, each performed subject to separate constraints and, in the case of QDT, often regularization^{17,23,28}. This two-step approach to QSE with an unknown detector is not only more resource intensive, owing to the two separate numerical optimizations, but also more likely to suffer from artefacts introduced from one or both of the separate optimization procedures³². Although ancilla-assisted detector characterization techniques might offer simpler post processing than standard QDT^{27,33}, they are limited by the available brightness of the requisite non-classical state³³. Furthermore, as in the case of standard QDT, a second optimization step to perform QSE using the reconstructed POVM elements is necessary.

Detector calibration by determination of data pattern set. To experimentally demonstrate the data pattern calibration and its subsequent application to state reconstruction for a detector with a large number of outcomes, we examine a BHD. This vital resource for continuous-variable quantum technologies is typically assumed to have an output that is proportional to the electric field quadrature of a well-defined spatial-temporal optical field mode^{9,11}. Indeed, balanced homodyne detection was used in the first quantum state and continuous-variable quantum process estimation experiments^{14,34}. Optical interference of a reference beam called the local oscillator with the unknown signal field to be examined defines the detection mode, as presented in Fig. 1b. The

balanced scheme suppresses the local oscillator technical noise and shot noise, allowing ultra-sensitive sampling of the signal.

The BHD is characterized by a set of probe states comprising 48 phase-averaged coherent states with varying amplitudes. The probe states are generated deterministically by attenuating and phase randomizing a laser beam, as shown in Fig. 1c. The use of phase-averaged probes to characterize the detector implies that the calibration field of view enables access to the photon number statistics of the unknown quantum states, which in the case of phase-invariant states constitutes complete QSE.

For each probe state σ_ξ , an ensemble of $K = 10^6$ optical pulses is measured sequentially by the BHD, yielding a set of voltages $\{V_1^{(\xi)}, V_2^{(\xi)}, \dots, V_K^{(\xi)}\}$ recorded by a fast oscilloscope. In the experiment, the probe state amplitudes $|\alpha_\xi|$ range from 0.17 to 2.24 in approximately even steps of 0.043. The frequency distribution $f_n^{(\xi)}$ of measurement outcomes n for state σ_ξ is formed by binning the voltage samples $\{V\}$ after rescaling (see Methods). Each frequency distribution consists of 151 bins, implying as many detector outcomes, which is more than an order of magnitude greater than any QDT experiment to date. The procedure is repeated for each probe state σ_ξ to give the detector data pattern set $\{f_n^{(\xi)}\}$, as shown in Fig. 2a, constituting the detector calibration. Note that no physical interpretation about the nature of the measurement outcomes is necessary in the FDP method^{24,25}.

Estimation of non-classical states using calibrated detector. Several non-classical photon number (Fock) states^{35–38} are

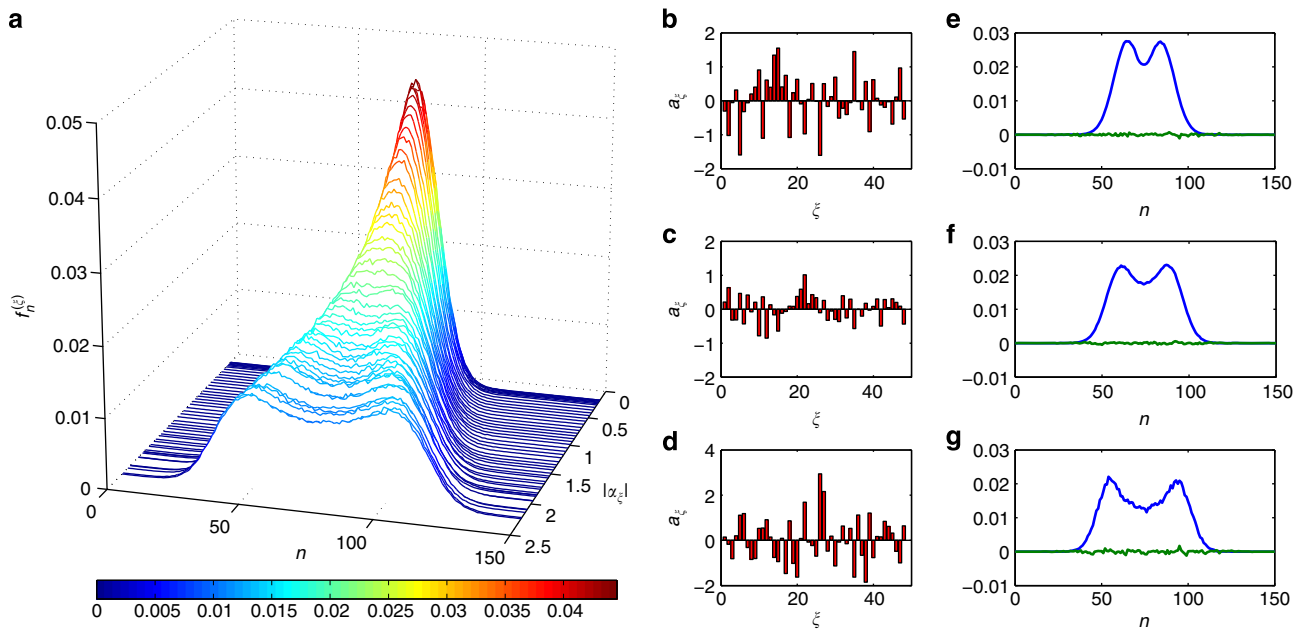


Figure 2 | Data pattern set and fitting of data patterns. (a) Data patterns $\{f_n^{(\zeta)}\}$ obtained for the set of 48 phase-averaged coherent state probes $\{\sigma_\zeta\}$ with $|\alpha_\zeta|$ ranging from 0.17 to 2.24. (b–d) Optimal coefficients $\{a_\zeta\}$ minimizing the functional defined in equation (3) for the one-, two- and three-photon Fock states, respectively. (e–g) Measured frequency distributions $f_n^{(\rho)}$ (blue curves) and residuals between fitted frequency distributions and measured frequency distributions $f_n^{(\rho)} - \sum_\zeta a_\zeta f_n^{(\zeta)}$ (green curves) for the one-, two- and three-photon Fock states, respectively, where index ζ is in the order of increasing probe state amplitude $|\alpha_\zeta|$. The latter gives a measure of the deviation between the measured and predicted frequency distributions, which is found to be within the statistical noise due to the finite number of measurements.

examined using the calibrated detector. The density matrices ρ are estimated by fitting the probe state data patterns $\{f_n^{(\zeta)}\}$ to the frequency distribution of measurement outcomes $f_n^{(\rho)}$ for heralded one-, two- and three-photon Fock states according to equation (3). The Fock states are generated by pulsed spontaneous parametric downconversion (see Methods) and measured by the BHD. Frequency distributions $f_n^{(\rho)}$ for each Fock state are obtained in the same manner as for the probe states, shown in Fig. 2. The functional defined in equation (3) is minimized for each state separately to determine the optimal set of coefficients $\{a_\zeta\}$, shown in Fig. 2b–d.

The reconstructed Wigner functions $W(X,P)$ and photon number statistics $P(n) = \langle n | \rho_{\text{fdp}} | n \rangle$ for the generated Fock states are shown in Fig. 3. To compare with the commonly used ML method for QSE, the same homodyne data that yield the frequency distributions $f_n^{(\rho)}$ are used in a ML QSE algorithm¹¹. Here, a POVM of the form $\{\pi_x\} = \{|X\rangle\langle X|\}$ and phase-invariant states are assumed, where $|X\rangle$ is the quadrature eigenstate with eigenvalue X (see Methods). The photon number distributions reconstructed with the ML estimation are shown in Fig. 3. The fidelity $F = \text{Tr}^2\left(\sqrt{\sqrt{\rho_{\text{fdp}}}\rho_{\text{ml}}\sqrt{\rho_{\text{fdp}}}}\right)$ between density matrices ρ_{fdp} and ρ_{ml} estimated by the FDP and ML methods for each Fock state is calculated, yielding fidelities $F_1 = 0.96 \pm 0.02$, $F_2 = 0.98 \pm 0.02$ and $F_3 = 0.92 \pm 0.02$ for the one-, two- and three-photon states, respectively. This agreement between FDP and ML approaches indicates that the assumed quadrature POVM used in the ML estimation is accurate within the field of view experimentally examined by the probe state calibration set and experimental uncertainties. It also provides a self-consistency check between the two methods, thus demonstrating the applicability of FDP method to characterization of many-outcome detectors and QSE.

Discussion

The ability to accurately calibrate the response of detectors is essential to the progress of quantum technologies. As quantum devices grow in size and complexity, so too will the measurement devices required for their operation and diagnosis. This necessitates the development of techniques to characterize increasingly elaborate detector responses. Standard QDT gives a complete global view of the detector and thus constitutes its characterization to all possible input states^{16,17,19,22,23}. Such calibration requires eliciting all measurement outcomes by probing the detector in large regions of input space that potentially have no overlap with states of interest to the experimenter. This leads to significant overheads in terms of experimental effort associated with preparing probe states and acquiring large data sets, and computational resources required to perform the numerical inversion of the data to extract the POVM set. Recent work has indicated that reconstruction of a restricted POVM set in a finite range may be possible²⁰, but further investigation on the probe state requirements and generalization to arbitrary detectors is needed. Furthermore, QSE with a well-calibrated detector using QDT requires an additional numerical inversion step that adds to the computational tasks for state estimation.

The data patterns approach to detector characterization and QSE represents a key conceptual shift in both detector calibration and state estimation. This approach provides a direct characterization of the detector response in a finite region of input state space in which we anticipate unknown states to exist. There is no numerical inversion associated with the detector characterization. The calibration consists only of the statistics of measurement outcomes, the data patterns, and in no time is the formal mathematical description of the detector, namely its POVM, revealed. Restricting the calibration region can greatly decrease the experimental and computational challenges, at the cost of limiting the domain over which the detector is characterized. The

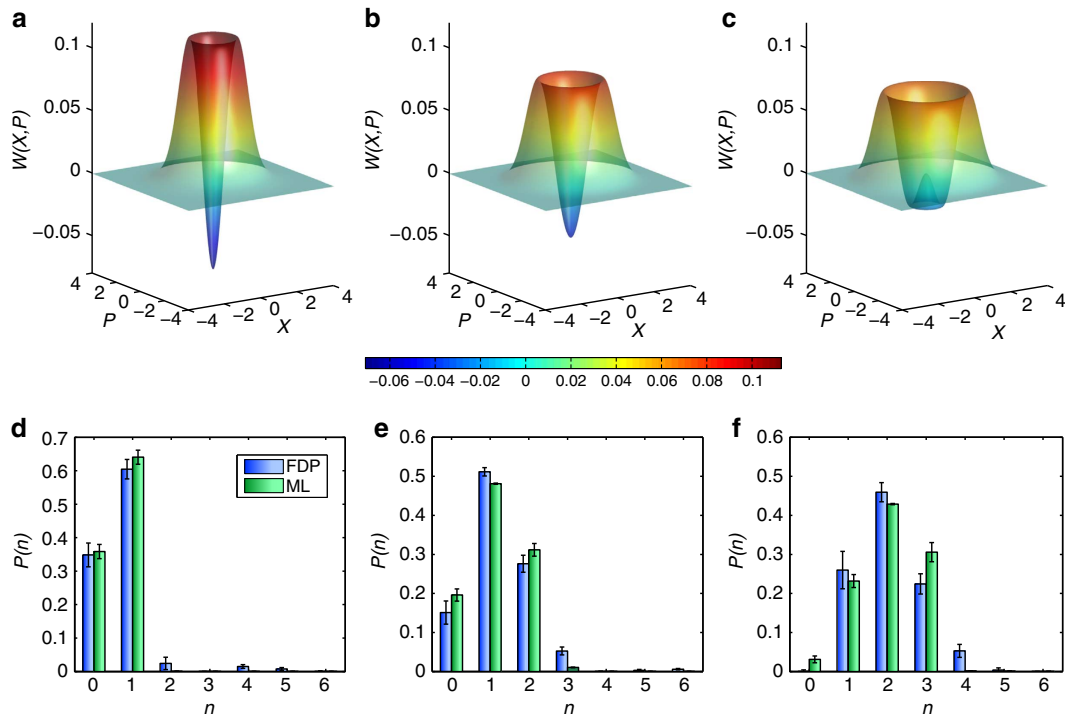


Figure 3 | Non-classical state reconstruction. Reconstructed Wigner functions $W(X,P)$ from FDP method (**a-c**) and photon number statistics $P(n)$ (**d-f**) from FDP (blue bars) and ML (green bars) methods for the (**a,d**) one-, (**b,e**) two- and (**c,f**) three-photon Fock states. The reconstructed Wigner functions exhibit negative values, thus indicating the non-classical nature of the reconstructed states. Error bars indicate one- σ confidence intervals and include both systematic and statistical sources of error for both the FDP and ML state reconstructions (see Methods).

single-step data processing for state estimation enables increased inversion speed.

Here we have presented an experimental demonstration of a novel method for quantum detector characterization and QSE by the FDP. This approach enables calibration of many-outcome detectors through direct, local measurement of the characteristic detector response to a set of probe states. The experimental calibration of a BHD and its subsequent use in reconstruction of non-classical Fock states presented here not only demonstrates successful implementation of this new detector characterization approach, but also goes an order of magnitude beyond any quantum detector characterization previously demonstrated. The FDP approach is easily adapted to a variety of measurement devices and the experimental implementation presented shows its viability for detectors with complex response. We anticipate that this approach to detector calibration and QSE will become a standard method to characterize measurement response in a local region of input space, adding to and complementing the QDT followed by QSE approach.

Methods

Balanced homodyne measurement. A time-domain BHD with a bandwidth of 80 MHz and signal-to-noise ratio of 14.5 dB is used to perform measurements of the probe and signal fields³⁹. For each incident optical pulse, the BHD generates a voltage pulse. The BHD voltage V is digitized by a computer-controlled digital storage oscilloscope. Drifts in the detector balance and gain are compensated by rescaling the measured voltage according to $V' = AV - B$. Rescaling parameters A and B are determined by acquiring pulses when the BHD input is blocked. Voltage samples with the input blocked are constrained to satisfy $\langle V' \rangle = C_1$ and $\text{var}(V') = \langle V'^2 \rangle - \langle V' \rangle^2 = C_2$, where C_1 and C_2 are constants, leading to the relations $A = \sqrt{(C_2/\text{var}(V))}$ and $B = A\langle V \rangle - C_1$. The local oscillator repetition rate is 80 MHz, whereas the probe state repetition rate is ~ 4 MHz. This enables continuous compensation for any drift³⁹. In the case of the ML state reconstruction, where a POVM is assumed, $C_1 = 0$ and $C_2 = 1/2$ is used, such that V' corresponds to a quadrature eigenvalue X for the case of a perfect BHD.

Probe state preparation. The phase-averaged coherent state probes are derived from a mode-locked Ti:Sapphire oscillator (Spectra-Physics Tsunami) operating at a central wavelength of 830 nm, full-width half-maximum bandwidth of 10 nm and repetition rate of 80 MHz, Fig. 1c. The beam is initially spatially filtered using a single-mode fibre and spectrally filtered using an interference filter (Semrock LL01-830-12.5), to match the spatial-spectral mode of local oscillator. A computer-controlled motorized half-wave plate followed by a Glan-Taylor polarizer and calibrated neutral density filters enables precise control of the probe state amplitude. Phase averaging is achieved by driving a piezoelectric translator on which one of the interferometer mirrors is mounted. The effective probe state amplitude $|\alpha_\xi|$ registered by the BHD is given by

$$|\alpha_\xi| = \sqrt{P_{\text{meas},\xi} \left(\frac{T}{R} \right) 10^{-\text{OD}_1 - \text{OD}_2} \nu^{-2} \frac{\lambda_0}{hc\nu}}, \quad (4)$$

where $P_{\text{meas},\xi}$ is the average power measured on the calibrated power meter (NIST-traceable Coherent FieldMaxII-TO power meter), $R(T)$ is the reflectivity (transmissivity) of the beam splitter, $\text{OD}_{1(2)}$ is the optical density of neutral density filter 1(2), ν is the laser repetition rate, λ_0 is the laser central wavelength and \mathcal{V} is the interference visibility between the local oscillator mode and probe state mode. The interference visibility is measured by removing the neutral density filters and directing one output of the 50:50 beam splitter used for balanced homodyne detection using a flip mirror to a fast photodiode that records the classical interference pattern as the phase is modulated. A calibrated spectrometer (Thorlabs CCS175) measures the central wavelength λ_0 . The probe state spectrum has a central value $\lambda_0 = 827.6$ nm. The laser repetition rate ν is measured using a high-precision frequency counter. The repetition rate is decreased by a pulse picker (APE) and was measured to be 3.997 MHz for the duration of the probe state measurement.

Fock state preparation. A two-mode squeezed vacuum state of the form $|\psi\rangle \approx \sqrt{1-\gamma^2}(|0,0\rangle + \gamma|1,1\rangle + \gamma^2|2,2\rangle + \gamma^3|3,3\rangle + O(\gamma^4))$, where γ is the squeezing parameter and $|n,m\rangle$ is a two-mode state with n (m) photons in the signal (trigger) mode, is generated by type II pulsed spontaneous parametric down-conversion in a bulk potassium di-hydrogen phosphate crystal⁴⁰. The signal and trigger modes are separated by a polarizing beam splitter. A spatially multiplexed detector comprising a fibre beam splitter network and three avalanche photodiodes (Perkin-Elmer SPCM-AQ4C) enables heralding of one-, two- and three-photon Fock states conditioned on registering one, two and three ‘clicks’, respectively, from the multiplexed detector³⁸. The heralded Fock state in the signal mode is combined with the local oscillator for performing balanced homodyne detection.

Reconstruction and uncertainty estimation. Minimization of functional equation (3) subject to constraints $\sum_{\epsilon} a_{\epsilon} = 1$ and $\sum_{\epsilon} a_{\epsilon} \sigma_{\epsilon} \geq 0$ can be formulated as a semi-definite programme. We used the YALMIP⁴¹ toolbox for MATLAB with the solver SDPT3 (ref. 42) to perform the minimization of equation (3).

The uncertainties in the state fidelities between ML and FDP approaches are estimated by taking into account both statistical and systematic sources of error. Statistical errors arise due to the finite number of measurement events used to generate data patterns and are given by $\sqrt{N_n}$ for each bin n with population N_n in the histograms, forming measurement outcome frequency distributions $f_n^{(\zeta)}$ and $f_n^{(\rho)}$. The bin width is chosen such that each bin is sufficiently narrow to adequately sample the underlying probability distribution²⁴. For the FDP state reconstructions, there are also errors originating from the estimates of P_{meas} and \mathcal{V} used to determine $|x_{\zeta}|$ for each probe state. Uncertainties of 5% in P_{meas} and 1% in \mathcal{V} are estimated, which give a total error for each $|x_{\zeta}|$ of 2.7%. For the ML state reconstructions, the primary source of error is the uncertainty in detector efficiency η_{hd} . This must be independently determined and explicitly taken into account in the ML estimation to compare with the FDP method, which automatically incorporates the detector efficiency. Monte Carlo simulation enables evaluation of the uncertainties for the estimated state density matrix elements and hence also the fidelities when comparing the FDP approach with the results from ML reconstruction. The Monte Carlo simulation takes into account statistical errors in the data patterns and state frequency distributions (as described above), as well as the uncertainty in the probe state amplitudes $|x_{\zeta}|$, which impacts the probe state density matrices $\{\sigma_{\zeta}\}$ and hence the estimated state ρ_{est} , equation (2).

References

- Zavatta, A., Parigi, V., Kim, M. S., Jeong, H. & Bellini, M. Experimental demonstration of the bosonic commutation relation via superpositions of quantum operations on thermal light fields. *Phys. Rev. Lett.* **103**, 140406 (2009).
- Yao, X. C. *et al.* Experimental realization of programmable quantum gate array for directly probing commutation relations of Pauli operators. *Phys. Rev. Lett.* **105**, 120402 (2010).
- Bachor, H. A. & Ralph, T. C. *A Guide to Experiments in Quantum Optics* (Wiley-VCH, 2004).
- Aasi, J. *et al.* Enhanced sensitivity of the LIGO gravitational wave detector by using squeezed states of light. *Nat. Photon.* **7**, 613–619 (2013).
- Bennett, C. H. & Brassard, G. in: *Proceedings of the IEEE International Conference on Computers, Systems and Signal Processing* 175–179 (IEEE Press, NY, USA, 1984).
- Becerra, F. E., Fan, J. & Migdall, A. Implementation of generalized quantum measurements for unambiguous discrimination of multiple non-orthogonal coherent states. *Nat. Commun.* **4**, 2028 (2013).
- Taylor, M. A. *et al.* Biological measurement beyond the quantum limit. *Nat. Photon.* **7**, 229–233 (2013).
- O'Brien, J. L., Furusawa, A. & Vuckovic, J. Photonic quantum technologies. *Nat. Photon.* **3**, 687–695 (2009).
- Leonhardt, U. *Measuring the Quantum State of Light* (Cambridge Studies in Modern Optics, Cambridge Univ. Press, 1997).
- Paris, M. & Řeháček, J. *Quantum State Estimation* (Lecture Notes in Physics vol. 649, Springer, 2004).
- Lvovsky, A. I. & Raymer, M. G. Continuous-variable optical quantum-state tomography. *Rev. Mod. Phys.* **81**, 299–332 (2009).
- Chuang, I. L. & Nielsen, M. A. Prescription for experimental determination of the dynamics of a quantum black box. *J. Mod. Opt.* **44**, 2455–2467 (1997).
- O'Brien, J. L. *et al.* Quantum process tomography of a controlled-NOT gate. *Phys. Rev. Lett.* **93**, 080502 (2004).
- Lobino, M. *et al.* Complete characterization of quantum-optical processes. *Science* **322**, 563–566 (2008).
- Anis, A. & Lvovsky, A. I. Maximum-likelihood coherent-state quantum process tomography. *New J. Phys.* **14**, 105021 (2012).
- Coldenstrodt-Ronge, H. B. *et al.* A proposed testbed for detector tomography. *J. Mod. Opt.* **56**, 432–441 (2009).
- Lundeen, J. S. *et al.* Tomography of quantum detectors. *Nat. Phys.* **5**, 27–30 (2008).
- Amri, T., Laurat, J. & Fabre, C. Characterizing quantum properties of a measurement apparatus: Insights from the retrodictive approach. *Phys. Rev. Lett.* **106**, 020502 (2011).
- Zhang, L. J. *et al.* Mapping coherence in measurement via full quantum tomography of a hybrid optical detector. *Nat. Photon.* **6**, 364–368 (2012).
- Brida, G. *et al.* Quantum characterization of superconducting photon counters. *New J. Phys.* **14**, 085001 (2012).
- Renema, J. J. *et al.* Modified detector tomography technique applied to a superconducting multiphoton nanodetector. *Opt. Express* **20**, 2806–2813 (2012).
- Natarajan, C. M. *et al.* Quantum detector tomography of a time-multiplexed superconducting nanowire single-photon detector at telecom wavelengths. *Opt. Express* **21**, 893–902 (2013).
- Zhang, L. J. *et al.* Recursive quantum detector tomography. *New J. Phys.* **14**, 115005 (2012).
- Řeháček, J., Mogilevtsev, D. & Hradil, Z. Operational tomography: fitting of data patterns. *Phys. Rev. Lett.* **105**, 010402 (2010).
- Mogilevtsev, D. *et al.* Data pattern tomography: reconstruction with an unknown apparatus. *New J. Phys.* **15**, 025038 (2013).
- Braunstein, S. L. & van Loock, P. Quantum information with continuous variables. *Rev. Mod. Phys.* **77**, 513–577 (2005).
- D'Ariano, G. M., Maccone, L. & Lo Presti, P. Quantum calibration of measurement instrumentation. *Phys. Rev. Lett.* **93**, 250407 (2004).
- Feito, A. *et al.* Measuring measurement: theory and practice. *New J. Phys.* **11**, 1–22 (2009).
- Hradil, Z. Quantum-state estimation. *Phys. Rev. A* **55**, R1561–R1564 (1997).
- Banaszek, K., D'Ariano, G., Paris, M. & Sacchi, M. Maximum-likelihood estimation of the density matrix. *Phys. Rev. A* **61**, 010304 (1999).
- Lvovsky, A. I. Iterative maximum-likelihood reconstruction in quantum homodyne tomography. *J. Opt. B Quantum Semiclass. Opt.* **6**, S556–S559 (2004).
- Blume-Kohout, R. Optimal, reliable estimation of quantum states. *New J. Phys.* **12**, 043034 (2010).
- Brida, G. *et al.* Ancilla-assisted calibration of a measuring apparatus. *Phys. Rev. Lett.* **108**, 253601 (2012).
- Smithey, D. T., Beck, M., Raymer, M. G. & Faridani, A. Measurement of the Wigner distribution and the density-matrix of a light mode using optical homodyne tomography—application to squeezed states and the vacuum. *Phys. Rev. Lett.* **70**, 1244–1247 (1993).
- Lvovsky, A. I. *et al.* Quantum state reconstruction of the single-photon Fock state. *Phys. Rev. Lett.* **87**, 050402 (2001).
- Zavatta, A., Viciani, S. & Bellini, M. Tomographic reconstruction of the single-photon Fock state by high-frequency homodyne detection. *Phys. Rev. A* **70**, 053821 (2004).
- Ourjoumtsev, A., Tualle-Brouri, R. & Grangier, P. Quantum homodyne tomography of a two-photon Fock state. *Phys. Rev. Lett.* **96**, 213601 (2006).
- Cooper, M., Wright, L. J., Söller, C. & Smith, B. J. Experimental generation of multi-photon Fock states. *Opt. Express* **21**, 5309–5317 (2013).
- Cooper, M., Söller, C. & Smith, B. J. High-stability time-domain balanced homodyne detector for ultrafast optical pulse applications. *J. Mod. Opt.* **60**, 611–616 (2013).
- Mosley, P. J. *et al.* Heralded generation of ultrafast single photons in pure quantum states. *Phys. Rev. Lett.* **100**, 133601 (2008).
- Löfberg, J. In *Computer Aided Control Systems Design, 2004 IEEE International Symposium on* 284–289 (2004).
- Toh, K. C., Todd, M. J. & Tütüncü, R. H. SDPT3—a MATLAB software package for semidefinite programming, version 1.3. *Optim. Method. Softw.* **11**, 545–581 (1999).

Acknowledgements

We are grateful for helpful discussions with M.G. Raymer and M. Barbieri. This work was supported by the University of Oxford John Fell Fund and EPSRC grant no. EP/E036066/1. BJS was partially supported by EPSRC grant EP/K034480/1. M.K. was supported by a Marie Curie Intra-European Fellowship no. 301032 within the European Community 7th Framework Programme.

Author contributions

M.C. and B.J.S. conceived the project. M.C. designed and performed the experiment. M.C. and M.K. performed modelling and data analysis, including code to implement the algorithm. All authors contributed equally to writing the manuscript.

Additional information

Competing financial interests: The authors declare no competing financial interests.

Reprints and permission information is available online at <http://npg.nature.com/reprintsandpermissions/>

How to cite this article: Cooper, M. *et al.* Local mapping of detector response for reliable quantum state estimation. *Nat. Commun.* 5:4332 doi: 10.1038/ncomms5332 (2014).



This work is licensed under a Creative Commons Attribution 4.0 International License. The images or other third party material in this article are included in the article's Creative Commons license, unless indicated otherwise in the credit line; if the material is not included under the Creative Commons license, users will need to obtain permission from the license holder to reproduce the material. To view a copy of this license, visit <http://creativecommons.org/licenses/by/4.0/>